JCTC Journal of Chemical Theory and Computation

Computational Studies of the X-Linked Inhibitor of Apoptosis Complex Formation with Caspase-9 and a Small Antagonist

George A. Kaminski*

Central Michigan University, Mount Pleasant, Michigan 48859

Received January 17, 2008

Abstract: Apoptosis is self-programmed cell death. The X-linked inhibitor of apoptosis (XIAP) is known to inhibit caspase proteins, the key players in apoptosis. When this happens, the cells become cancerous as they cannot die naturally. XIAP inhibitors are often overexpressed in cancer tissue. Presented in this article are the results of simulations of XIAP-caspase and XIAP-antagonist complexes. It has been previously established experimentally that low intensity ultrasound promotes apoptosis and increases the therapeutic effect of some XIAP-caspase interaction antagonists. The resulting calculated complex formation energies produced in this work were used with a simple multiscale model as an example of applying such energetic results for estimating the effects of ultrasound on these complexes. The microscopic simulations have been carried out with molecular mechanics employing an all-atom description of the molecules with the OPLS-AA and polarizable force field (PFF) formalisms. It has been determined that the interaction energies in the XIAP-caspase-9 pair with both OPLS and PFF are roughly the same and in the 30–40 kcal/mol range, while PFF predicts a higher magnitude of energy of the XIAP-antagonist complex formation (ca. 100 kcal/mol vs ca. 40 kcal/mol), thus probably being more adequate in reproducing the inhibition abilities of this low molecular weight antagonist. The presented study of the ultrasound effect leads to the conclusion that it is most likely based on the cavitation accompanying the ultrasound irradiation of the cells and not on a simple frequency resonance, as was suggested by some authors.

I. Introduction

A. Apoptosis As a Natural Anticancer Mechanism, Caspase Proteins, X-Linked Inhibitor of Apoptosis. Apoptosis is a specific type of self-induced cell death.[1] Alteration of apoptosis pathways can lead to its being underpresent, which causes the cells to become "immortal" (cancer).[1b] This is why recently there has been much attention directed toward understanding apoptosis and its reactivation after inhibition, especially in the area of cancer research.[2]

Apoptosis is executed by caspases, a family of cystein proteases. The critical involvement of caspases in apoptosis has been documented and discussed in a number of works.[1,2] Clearly, inhibition of caspases leads to a failure of apoptosis. The Inhibitors of Apoptosis (IAP) are a family of proteins which strongly interact, bind, and inhibit caspases. XIAP (or X-linked inhibitor of apoptosis) is one of such molecules receiving much attention recently.[3] Each XIAP protein contains copies of the 80 residue baculoviral IAP repeat (BIR). Each BIR domain has a distinct function. For example, BIR3 of XIAP efficiently inhibits caspase-9 protein. The BIR3 domain of XIAP captures caspase-9 in its inactive conformation and prevents activation.[1b]

Thus, the XIAP effectively stops apoptosis. Disruption of the XIPA (BIR3) – caspase-9 complex (inhibition of XIAP) is viewed as a way to induce apoptosis in cancer cells and to work as an antitumor agent. A number of experimental studies of possible pro-apoptosis agents, including Smac/DIABLO, peptides similar to Smac/DIABLO, and small molecules, have been undertaken.[4] Promoting apoptosis is a valid and actively pursued target in current cancer research.

* Corresponding author e-mail: kamin1ga@cmich.edu.

10.1021/ct8000188 CCC: $40.75
Published on Web 03/29/2008

This article is intended to make a molecular modeling contribution in the area of studying apoptosis inhibition.

B. Simulations of Intermolecular Interactions – Fixed Charges and Polarizable Force Fields. One of the most common approaches in simulation of proteins is the fixed-charges model. In this case, the electrostatic interactions between particles are represented by attraction or repulsion between constant predetermined Coulomb charges assigned to the atomic sites. This scheme is implemented in such widely used force fields as AMBER,[14] MMFF,[15] and OPLS-AA.[16] While this approach usually predicts the structure of biological systems and the relative binding energies rather well, and the computational efficiency is high, there are certain limitations to the technique. Since the Coulomb charges on atoms do not change in the course of simulations, there is no way the simulated electrostatics can adequately respond to a changing electrostatic environment. For example, when a molecule is immersed in a polar solvent, such as water, it usually becomes more polar (a water molecule in gas phase has a dipole moment of ca. 1 Debye lower than the same molecule in pure liquid water[17]). If a force field utilizing permanent fixed charges is parametrized to reproduce liquid-state properties, it will inevitably be overpolarized for gas-phase or other low dielectric constant media. This is why absolute binding energies in gas phase can be overestimated by fixed-charges force fields by as much as 2.5 kcal/mol even for small molecules.[18] It is therefore highly desirable to have a polarizable electrostatic model, which can readjust as the environment changes. In this case, magnitudes of the charges can change or point electrostatic dipoles are induced. A number of polarizable force fields have emerged in recent years, with the scope of the applications ranging from neat liquids to protein–ligand complexes in solutions and computing absolute acidity constants.[19,20]

Since the purpose of the presented work is directly dependent upon estimating binding energies, it is natural to assume that the explicit treatment of electrostatic polarization could be inportant. This is why this work was done with using both fixed-charges OPLS-AA force field[16,21] and a recently developed polarizable force field for proteins and small molecules.[18,19e] Comparison of the results is aimed at identifying the situations in which employing polarizable force fields is critical.

C. Application of Low-Intensity Ultrasound As an Apoptosis-Promoting Technique. Uses of ultrasound in medical applications are numerous and range from imaging in diagnostics to ultrasound treatments of tumors.[5–10] Effects of low-intensity ultrasound are less well studied than those of the high-intensity one, but they are nevertheless quite promising, especially in the area of cancer research. For example, death rate of human ovarian carcinoma cells have been reported to increase as a result of ultrasound sonification, while the energy directly associated with the ultrasound itself was clearly not sufficient to kill them.[11] Apoptosis in human leukemic cells can be induced by low-energy ultrasound, which suggests new ways of anticancer therapy.[10] Enhancement of chemotherapy by sonification has also been reported. Exposure to ultrasound enhances cytotoxicity of anticancer chemicals to cancer cells. As a result, the dosage of a drug can be reduced and a patient's tolerance to chemotherapy improved.[7] Ultrasound can synergize the effects of adriamycin, cisplatin, 5-fluoraurcail, arabinosyl cytosine, boron hydrochloride monohydrate, diazoquononem, and 4′-O-tetrahydropyranyladriamicyn.[7] The synergy has been confirmed in ovarian cancer, breast cancer, cervical cancer, and leukemia.

While the apoptosis inducing effect of ultrasound sonification has been established experimentally, the exact mechanism of this process still remains to be understood. Currently, three hypotheses have been put forward.[7] The first one suggests that the ultrasound irradiation causes conformational shifts, such as, for example, turning an inactive form of caspase proteins into active ones. The second hypothesis is the resonant frequency one, which states that the frequency of the irradiating ultrasound is close to the frequency of, for example, XIAP-caspase bonding. Thus, the ultrasound directly destroys the harmful caspase inhibition complex in a targeted manner. Finally, the third hypothesis is that the destruction of the cancer cells is caused by cavitation. Cavitation is a phenomenon which accompanies ultrasound propagation in liquids, such as water. An ultrasound wave creates zones of increased and decreased pressure. When the pressure is sufficiently decreased, a gas bubble emerges. Then the pressure increases again, and the bubble collapses. This cycle is repeated with the frequency of the ultrasound. The collapse of the air bubbles creates shock waves, and the pressure in these waves can reach as high as 40–60 kbar.[12,13] Therefore, the pressure range in the medium can greatly exceed the nominal ultrasound wave pressure amplitude of ca. 1.5 kbar.

The work presented in this manuscript explores the frequency resonance and cavitation action hypotheses at the microscopic level to cast light on the mechanism of the low-intensity ultrasound-induced apoptosis in cancer cells.

The remainder of the paper is organized as follows. Section II describes the methodology involved in computing microscopic protein–ligand interaction energies and the mechanistic model used to assess the effect of ultrasound upon the complex formation. Section III presents results of the calculations. These are followed by conclusions in Section IV.

II. Methods

A. Calculating Intermolecular Interaction Energies. First, interaction energies of the BIR3 domain of XIAP with the caspase-9 protein and a small molecular antagonist were calculated using both OPLS-AA and polarizable force field (PFF). The initial geometries of the complexes were taken from Protein Data Bank structures 1NW9 and 1TFQ, respectively. Hydrogen atoms were added to the structures using the Maestro program.[22] Then each complex was truncated so that only those residues with at least one atom within a cutoff distance of 7.5 Å of any atom of the other molecule in the complex were considered and all the other residues discarded. The small antagonist[23] shown in Figure 1 was not truncated in any way.

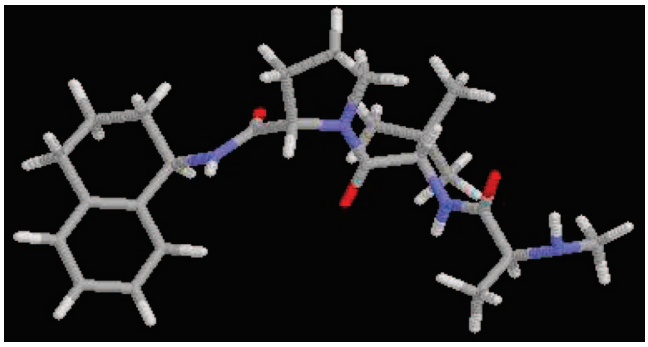

Figure 1. Antagonist to the XIAP-caspase-9 interaction.

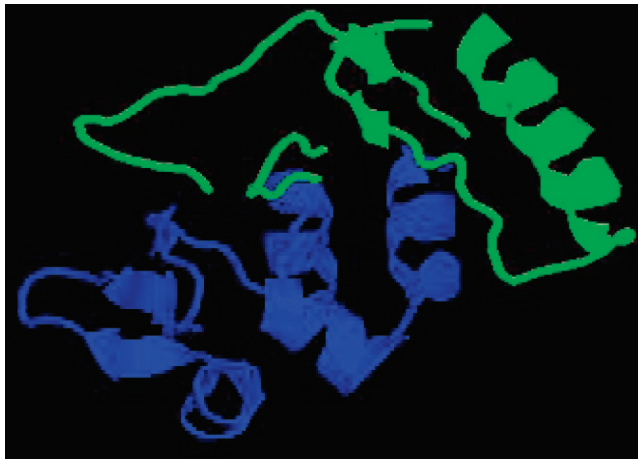

Figure 2. Explicitly modeled part of the XIAP-BIR3 interacting with caspase-9 protein. Residues present: chain A (blue): Leu256–Arg258, Val279–His346; chain B (green): Tyr153, Gln240–Gly248, Ala316–Gln320, Ser333–Thr347, Asp379–Lys410; Zn^{2+} ion (not shown).

Figures 2 and 3 demonstrate parts of the molecules included in simulations.

For each of the two complexes, a series of energy minimizations was performed. The parts of the complexes (chains A and B in the first case, chain A and the ligand in the second one) were moved with respect to each other prior to the optimizations in order to obtain interaction energy as a function of distance between the parts. The parts were displaced along the line passing through the centers of masses of the parts in their original full form (as in the PDB files, not truncated). Geometry of the ligand (red in Figure 3) was fixed. For all the protein parts, backbone geometry was fixed in the course of the energy minimizations, and the side chains were completely flexible. Interaction energies were computed using the OPLS-AA force field[16,21] and, in separate runs, the complete polarizable force field for proteins[19e] and polarizable force field for small molecules.[18] Geometry optimizations were performed in continuum PBF solvent corresponding to water for the polarizable force field[19e] and the standard IMPACT SGB model in the OPLS-AA calculations. IMPACT software suite was used for all the energy minimizations.[24] A conjugate gradient technique was employed with the convergence criterion for the final energy gradient set to 0.05 kcal/mol/Å.

After the dependence of the interaction energies on the distance between the parts of the complexes was obtained as described above, it was used in the mechanistic model introduced below to determine the effect of ultrasound irradiation on the XIAP-BIR3 complexes with caspase-9 and the small molecular antagonist.

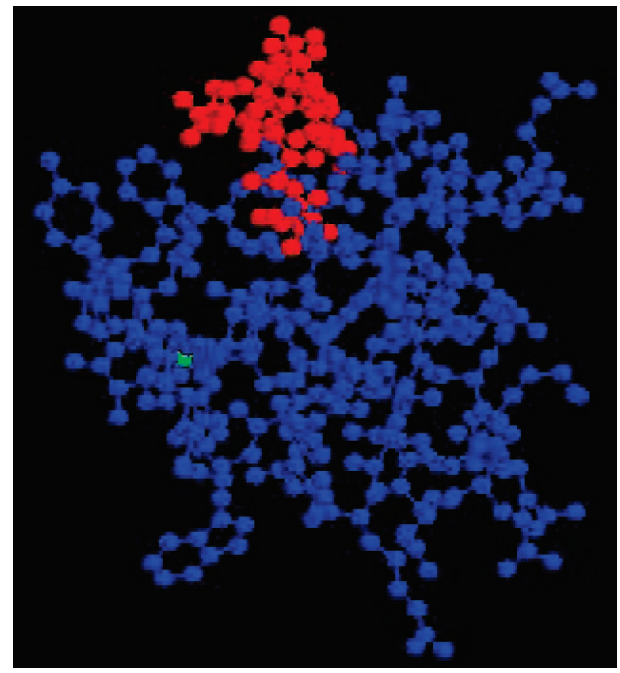

Figure 3. Explicitly modeled part of the XIAP-BIR3 interacting with the small antagonist. Residues present: chain A (blue): Tyr277–Tyr324; complete ligand (red); Zn^{2+} ion (green).

B. Force Fields. We have used both a polarizable force field (PFF) and a fixed-charges OPLS-AA. The procedure for building the PFF has been described elsewhere.[18] In the essence, the electrostatic interactions are represented by interactions of fixed charges and inducible point dipoles with each other. Fourier series were employed for the torsional energy and harmonic bond stretching and angle bending parameters were used.

In case of the fixed-charges OPLS force field, the key difference was that the nonbonded part was calculated as

$$E_{\mathrm{nb}} = \sum_{i<j} \left[q_i q_j e^2 / r_{ij} + 4\varepsilon_{ij}\left(\sigma_{ij}^{12}/r_{ij}^{12} - \sigma_{ij}^{6}/r_{ij}^{6}\right)\right] f_{ij} \qquad (1)$$

The summation runs over all the pairs of atoms $i < j$ on molecules A and B or A and A for the intramolecular interactions. Moreover, in the latter case, the coefficient f_{ij} is equal to 0.0 for any *i-j* pairs connected by a valence bond (1–2 pairs) or a valence bond angle (1–3 pairs). $f_{ij} = 0.5$ for 1,4-interactions (atoms separated by exactly 3 bonds) and $f_{ij} = 1.0$ for all the other cases. Standard OPLS-AA parameters were used.

C. Mechanistic Model for the Effect of Ultrasound Irradiation on the Protein–Ligand Complexes. The data from the intermolecular interactions simulations were used in a simple mechanistic model which has been devised to qualitatively estimate effects of ultrasound on the complexes in hand. While other mechanistic models had been proposed before,[25] none of them were combined with an explicit all-atom simulations to provide a detailed description of processes in a small protein–ligand complex. The

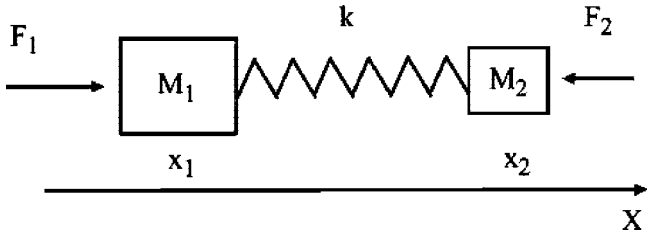

Figure 4. Mechanistic model for the protein–ligand complex.

model is somewhat crude, but it permits the drawing of conclusions in qualitative agreement with the available experimental data. The protein–ligand complex is schematically shown in Figure 4.

The interacting protein and ligand are represented as masses M_1 and M_2 located at one-dimensional positions x_1 and x_2 and connected by a spring with a constant k. In addition, the masses are experiencing external forces $F_1 = P \cdot A_1$ and $F_2 = P \cdot A_2$, where P is the external pressure and A_1 and A_2 are effective areas of the molecules. $A = \pi d^2/4$, where d is the largest distance between two atoms in a molecule. In the presence of ultrasound, $P = P_0 \cos(\omega t)$, where P_0 and ω are the amplitude and angular frequency of the ultrasound wave, and t stands for time. Then the equations of motion for the masses 1 and 2 are

$$\begin{aligned} M_1\ddot{x}_1 &= -k(x_1 - x_2) + F_1 \\ M_2\ddot{x}_2 &= -k(x_2 - x_1) - F_2 \end{aligned} \tag{2}$$

Dividing each equation by the corresponding mass and subtracting the second one from the first

$$\ddot{x}_1 - \ddot{x}_2 = \left(-\frac{k}{M_1} - \frac{k}{M_2}\right)(x_1 - x_2) + \frac{F_1}{M_1} + \frac{F_2}{M_2} \tag{3}$$

We are only interested in relative motion of the molecules, thus we can disregard the result of adding the eqs 2 describing the motion of the center of mass. Introducing a new variable $y = x_1 - x_2$

$$\ddot{y} = -\frac{k(M_1 + M_2)}{M_1 M_2} y + \left(\frac{F_1}{M_1} + \frac{F_2}{M_2}\right) \tag{4}$$

Using the reduced mass $\mu = M_1M_2/(M_1+M_2)$ and introducing $a(t) = a_0\cos(\omega t) = F_1/M_1 + F_2/M_2 = P \cdot A_1/M_1 + P \cdot A_2/M_2 = (A_1/M_1 + A_2/M_2) \cdot P = (A_1/M_1 + A_2/M_2) \cdot P_0 \cos(\omega t)$, thus $a_0 = P_0 \cdot (A_1/M_1 + A_2/M_2)$, and, from eq 4

$$\ddot{y} + \frac{k}{\mu} y = a_0 \cos(\omega t) \tag{5}$$

or, with $k/\mu = \omega_0^2$

$$\ddot{y} + \omega_0^2 y = a_0 \cos(\omega t) \tag{6}$$

Equation 6 represents the classical problem of driven oscillatory motion. The solution (after a certain equilibration time) is

$$y = \frac{a_0}{\omega_0^2 - \omega^2} \cos\omega t) \tag{7}$$

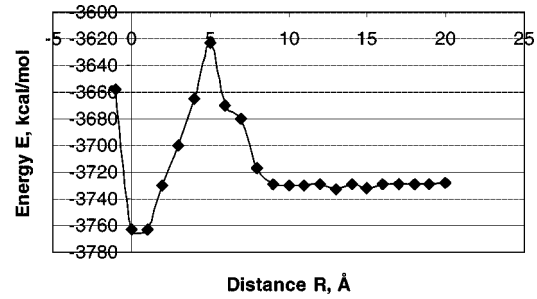

Figure 5. Energy E of XIAP-BIR3 interaction with caspase-9 as a function of the distance R between the molecules. Computed with the OPLS-AA force field.

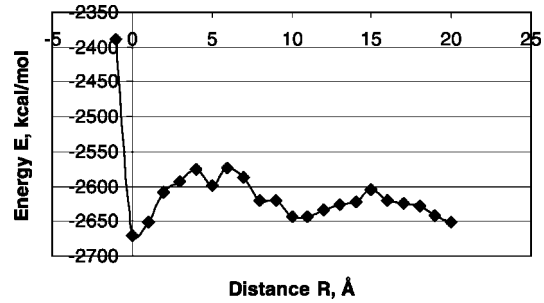

Figure 6. Energy E of XIAP-BIR3 interaction with caspase-9 as a function of the distance R between the molecules. Computed with the polarizable force field (PFF).

Therefore, the amplitude of the forced motion of the protein and ligand with respect to their equilibrium positions in the complex is

$$y_0 = \frac{a_0}{\omega_0^2 - \omega^2} = P_0 \frac{A_1/M_1 + A_2/M_2}{k/\mu - (2\pi\nu)^2} \tag{8}$$

where ν is the linear frequency of the ultrasound.

Therefore, all we have to do is to (i) calculate the k and frequency $w_0 = (k/\mu)^{1/2}$ of the protein–ligand complex (using the energy vs distance dependence obtained as outlined above and assuming quadratic behavior near the energy minimum) and (ii) find the amplitude of oscillation for the complex y_0 and (iii) check if the complex would be destroyed–or considerably weakened–with such a deviation from the equilibrium distance. Again, the model is crude, but it permits qualitative understanding of the process of ultrasound interaction with the protein–ligand complexes.

III. Results and Discussion

A. Intermolecular Interaction Energies. Interaction energies of the BIR3 domain of XIAP with the caspase-9 protein and a small molecular antagonist were calculated as a function of the separation distances between the XIAP and caspase-9 or the antagonist, as described in section II above. Let us first consider the XIAP-caspase-9 complex. Figures 5 and 6 show these energy profiles calculated with the OPLS-AA and PFF force fields, respectively.

For these and for all the following graphs the point $R = 0$ corresponds to the intermolecular distance found in the original PDB file, and the simulation points are separated

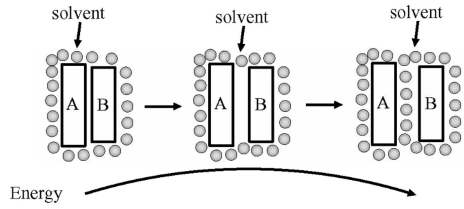

Figure 7. Schematic illustration of the total energy behavior in the process of separating interacting molecules A and B in solution.

by 1.0 Å distance. The lines added to the graphs are simply smoothened lines connecting the points and not a specific interpolation.

Several observations can be made from the above graphs. First of all, both OPLS-AA and PFF predict the intermolecular interaction energy minima at the same point as the experimentally reported structure in the 1NW9 PDB file (within the 1.0 Å precision). Second, the polarizable force field predicts a much steeper growth of the energy for distances shorter than at the equilibrium.

Both Figures 5 and 6 share one important characteristic. As the molecules start getting separated, the energy first increases by several tens of kcal/mol and then drops down, with the total energy of the binding of ca. 30–40 kcal/mol. This effect is well known and is schematically shown in Figure 7. When macromolecules A and B form a complex in solution (left), each of them loses some solvation energy as a part of its surface is not accessible to the solvent. At the same time, some favorable interaction energy is gained because of the intermolecular attractions. When the molecules start separating (center), this dimerization energy becomes less negative, as the distance between the molecules increases. At the same time, the solvent still cannot penetrate the empty space between the molecules A and B, and thus the solvation energy does not become more negative.

Finally, when the molecules are sufficiently far away from each other (right), the solvent can completely solvate both molecules, and the total energy of the complex goes down again, since the lost dimerization energy is at least partially compensated by the energy of solvation. Therefore, the whole process requires transition over an activation barrier. This behavior is precisely what is reproduced by our energy minimizations in continuum solvent, as shown in Figures 5 and 6.

Only a relatively small part of the potential energy curve, with the distances shorter than ca. 4–5 Å, is actually relevant for our efforts to find the harmonic force constant k of the XIAP-caspase complexes as approximated by Figure 4 and consequent equations. Figures 8 and 9 demonstrate the energy-distance dependences for these areas as computed with the OPLS-AA and PFF, respectively.

These two graphs are shown in the same scale, and it can be immediately noticed that the general potential well shape is rather similar with both force fields, even though the approximated curvatures are somewhat different.

In this case, the lines shown on the graphs are results of a polynomial fit. To account for the unharmonicity and to efficiently separate the quadratic form, a fourth degree

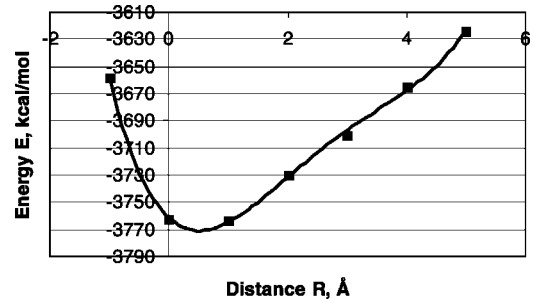

Figure 8. Energy E of the XIAP-BIR3 interaction with caspase-9 as a function of the distance R between the molecules (for small distances). Computed with the OPLS-AA force field.

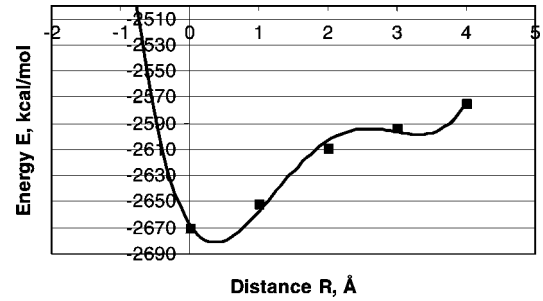

Figure 9. Energy E of the XIAP-BIR3 interaction with caspase-9 as a function of the distance R between the molecules (for small distances) with the polarizable force field (PFF).

polynomial was used in each case. The best-fit polynomial for the OPLS-AA force field was $E(R) = 1.1684R^4 - 12.844R^3 + 48.604R^2 - 40.237R - 3761.4$. The PFF polynomial was $E(R) = 6.4187R^4 - 53.7R^3 + 138.1R^2 - 80.635R - 2667.7$. The nonzero linear terms are employed to account for a slight difference between the positions of the experimental ($R = 0$) and calculated energy minima.

The force constants k, as computed from the above equations and the general harmonic formula $E(R) = ½\, kR^2$, are 97.21 kcal/(mol·Å^2) and 276.2 kcal/(mol·Å^2) or 67.58 N/m and 192.0 N/m as computed with the OPLS-AA and PFF, respectively. These values will be used in the next subsection to estimate the effect of an ultrasound irradiation upon the complexes.

Let us now consider the second complex–the one between the BIR3 domain of XIAP and an antagonist to the XIAP-caspase interaction.[23] First of all, it should be pointed out that a successful antagonist has to have a strong interaction energy with the XIAP molecule, and this trend should be reflected in the computational results. Figures 10 and 11 show the dependence of the XIAP-antagonist binding energy on the distance between the two molecules. The line connecting the data points is a smooth connecting line, and $R = 0$ corresponds to the experimentally observed PDB structure (1TFQ).

The following observations can be made here. First, both OPLS-AA and PFF predict the global energy minimum to be at a distance 1.5–2.0 Å shorter than in the PDB structure. Second, the PFF energy is growing steeper than the OPLS-AA one as the molecules get closer to each other–just like

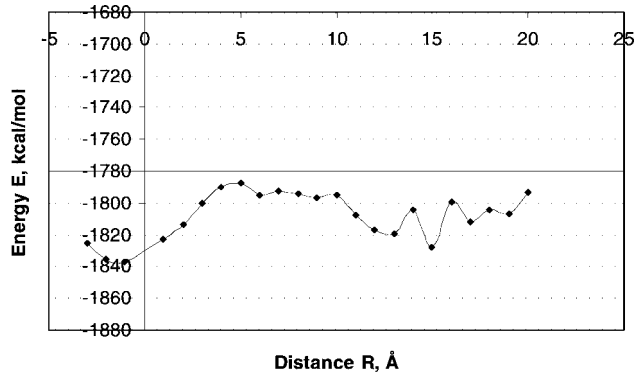

Figure 10. Energy *E* of the XIAP-BIR3 interaction with the antagonist (shown in Figure 1)[23] as a function of the distance *R* between the molecules. Computed with the OPLS-AA force field.

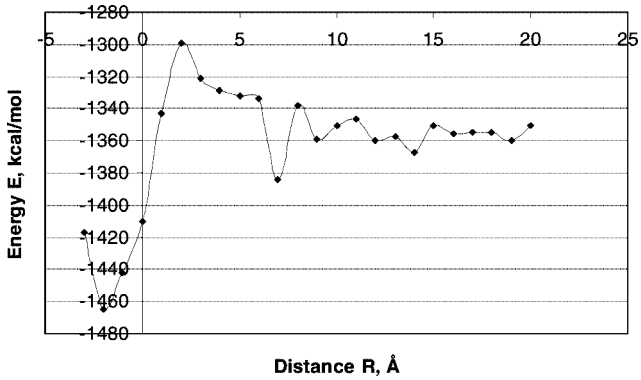

Figure 11. Energy *E* of the XIAP-BIR3 interaction with the antagonist (shown in Figure 1) as a function of the distance *R* between the molecules. Computed with the polarizable force field (PFF).

in the case of the XIAP-caspase complex. Third, the general trend of the energy going up and them down as the molecules are separated is still preserved in this case. However, there is a major difference between the PFF and OPLS-AA performance in this case. The binding energy for the complex is about 100 kcal/mol with the former and ca. 40 kcal/mol with the latter. Therefore, PFF predicts the antagonist to be more successful than the OPLS, which only indicates a binding energy as roughly the same as for the XIAP-caspase complex. This pronounced difference can be attributed to the ability of the polarizable force field to react adequately to changes in the electrostatic environment and to interfaces between areas with different dielectric constants (water–protein–ligand). This ligand is smaller than the caspase-9 protein, and thus a sharper adjustment is required, with the molecules experiencing influences of all the three areas. This is why the advantage of the PFF model (more favorable binding energy) seems to be more noticeable in this case of a relatively small molecule bound to the XIAP protein.

Let us now consider the energy-distance dependence for the small distances and derive the strength constants *k* for the complex. The energy dependence on the intermolecular distances is shown in Figures 12 and 13 for the OPLS-AA and PFF, respectively.

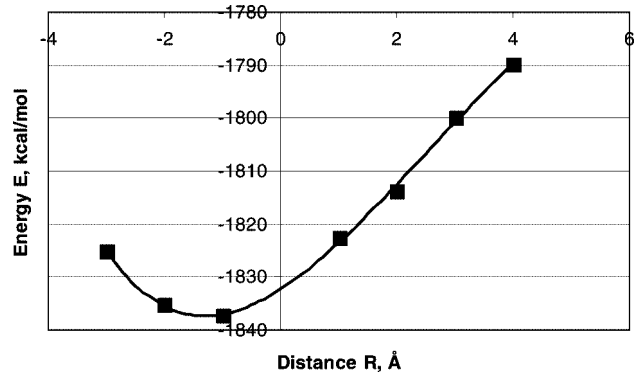

Figure 12. Energy *E* of the XIAP-BIR3 interaction with the antagonist (shown in Figure 1)[23] as a function of the distance *R* between the molecules (for small distances). Computed with the OPLS-AA force field.

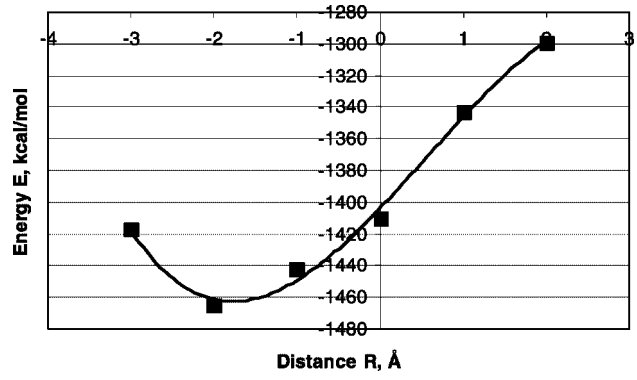

Figure 13. Energy *E* of XIAP-BIR3 interaction with the antagonist (shown in Figure 1)[23] as a function of the distance *R* between the molecules (for small distances). Computed with the polarizable force field (PFF).

These graphs are given in different energy scales, as the overall energy changes are greater with the polarizable force field. The lines on the graphs represent fourth degree polynomial fits produced for finding the quadratic part of the energy-distance relationship. The best-fit fourth degree equations were produced in the same way as for the XIAP-caspase complexes. The equations for the OPLS-AA and PFF curves are, respectively, $E(R) = 0.0128R^4 - 0.3361R^3 + 2.0327R^2 + 7.0849R - 1832.3$ and $E(R) = 0.0235R^4 - 3.5619R^3 + 5.858R^2 + 55.013R - 1403.6$, where *E* is in kcal/mol and *R* is in Angstroms. This leads to the strength constant *k* values computed with the OPLS-AA and PFF being 4.066 kcal/(mol·Å^2) and 11.72 kcal/(mol·Å^2), respectively. These values translate into 2.827 N/m and 8.145 N/m. As could be expected, the PFF strength constant is higher, and the difference is greater than for the XIAP-caspase case, for which the OPLS-AA and PFF results are more similar.

The values of the computed *k* constants are shown together in Table 1.

B. Ultrasound Irradiation Effect on the Strength of the Complexes of XIAP-BIR3. As all the required values of *k* have been obtained as described above. Let us now list the other parameters required in eq 8. Once all the values are known, this equation can be used to determine the amplitudes of the molecular motion in the protein–ligand complexes and thus estimate their stability.

Table 1. Values of the Strength Constant *k* for the Protein−Ligand Complexes Computed with the OPLS-AA and PFF Force Fields

	XIAP-BIR3 with caspase-9		XIAP-BIR3 with the small antagonist	
complex/method	kcal/(mol·Å^2)	*N*/m	kcal/(mol·Å^2)	*N*/m
OPLS-AA	97.21	67.58	4.066	2.827
PFF	276.2	192.0	11.72	8.145

Table 2. Masses of the Molecules (in amu), Diameters (in Å), and Area ($A = \pi d/4$, in A^2)

value/molecule	mass	diameter	area
caspase-9	30434.13	64.1	3227.05
XIAP-BIR3	13474.28	66.4	3462.79
small antagonist	442.59	16.5	213.82

The masses and the diameters (estimated as the largest atom−atom distance within the molecule) for the caspase-9, XIAP-BIR3, and the antagonist from the PDB 1TFQ are given in Table 2.

The following typical values of the ultrasound frequency and pressure amplitude are assumed: 0.68 MHz and 1.5 MPa.

Having obtained and chosen all these input data, let us now apply eq 8 to find the maximum displacements of the molecules from their equilibrium positions. For the XIAP-caspase complex, the values of y_0 for the OPLS-AA and PFF are, respectively, $y_0(\mathrm{OPLS}) = 7.525 \times 10^{-13}$ m $= 0.007525$ Å and $y_0(\mathrm{PFF}) = 2.649 \times 10^{-13}$ m $= 0.002649$ Å. For the XIAP-antagonist complex, eq 8 gives the amplitudes of displacements of the molecules with respect to each other of $y_0(\mathrm{OPLS}) = 1.683 \times 10^{-12}$ m $= 0.01683$ Å and $y_0(\mathrm{PFF}) = 5.841 \times 10^{-13}$ m $= 0.005841$ Å.

It is quite obvious that such small displacements will not be able to change the stability of the complexes in any significant degree. The reason for this result is in the huge differences between the frequency of the ultrasound and the vibrational frequencies of the complexes. These frequencies, entering as $\omega^2 = k/\mu$ into eq 8, are as follows. For the XIAP-caspase complex, the OPLS-AA frequency is $\omega = 2.088 \times 10^{12}$ rad/s or 3.222×10^{11} Hz. The PFF results for this complex are $\omega = 3.519 \times 10^{12}$ rad/s or 5.600×10^{11} Hz. For the XIAP-antagonist complex, the OPLS-AA frequency is $\omega = 1.993 \times 10^{12}$ rad/s or 3.172×10^{11} Hz, and the PFF frequency is $\omega = 3.383 \times 10^{12}$ rad/s or 5.384×10^{11} Hz. Clearly, such a huge difference in the frequencies does not allow the complexes to be anywhere near the resonance while irradiated with the ultrasound.

The above results permit a clear and definite conclusion that the simple frequency resonance hypothesis cannot explain the removal of the apoptosis inhibition by irradiating a tissue with low-intensity ultrasound. It is known however, that a difference in the frequencies can be compensated by using a larger magnitude of the driving oscillations. In this case, we are talking about oscillations of the pressure. It has been shown, both experimentally and theoretically, that irradiation of a liquid with low-intensity ultrasound leads to cavitation, and the bubbles present as a result of cavitation collapse releasing shock waves with pressures of up to 40–60 kbar.[12,13] This leads to the actual pressure amplitude being increased from the nominal 1.5 MPa to ca. 50 kbar $= 5 \times 10^9$ Pa $= 5000$ MPa. The variation of pressure is no longer obeying the exact $\cos(\omega t)$ form, but let us assume that eq 8 is still valid for the purpose of estimating the effect. In this case, the amplitude of motion of the caspase-9 and XIAP-BIR3 molecules with respect to each other are 25.1 Å with the OPLS-AA and 8.83 Å with the polarizable force field. The displacement of the XIAP-BIR3 and small antagonist molecules are 56.1 Å with the OPLS-AA and 19.5 Å. Therefore, all the complexes are effectively destroyed if we consider the cavitation resulting from the ultrasound irradiation. We can thus assume that the effect of the ultrasound on the apoptosis reactivation is much more likely to be rooted in the accompanying cavitation and definitely not in the simple frequency resonance. All the calculated displacements and frequencies are shown together in Table 3.

This first of the above results is not a big surprise. A typical ultrasound frequency is much lower than a typical molecular-scale oscillations frequency. Therefore, one could guess that resonance is not responsible for destruction of these molecular complexes without carrying out the detailed molecular calculations described above. However, these calculations are needed to assess the displacement resulting from the ultrasound irradiation quantitatively. A difference in frequencies in driven oscillations can be compensated by a difference in amplitudes–the typical amplitude of ultrasound oscillations is by far greater than the few angstroms of separation needed to destroy a molecular complex. Whether the complex will be destroyed or not is determined by the balance of the unfavorable difference in the frequencies and favorable difference in the amplitudes. And the detailed calculations are needed to quantitatively study this balance. Therefore, our conclusion that, in the presence of cavitation, the ultrasound irradiation is sufficient for destruction of the XIAP complexes, is not trivial and could not be made a priori without the quantitative assessment.

Table 3. Frequences of the One-Dimensional Complex Vibrations (ω in rad/s, N in Hz) and Amplitudes of Changes in the Intermolecular Distances, Å

	frequency		amplitude of displacement	
value/complex	ω	ν	w/o cavitation	with cavitation
XIAP-caspase,OPLS	2.088×10^{12}	3.322×10^{11}	0.007525	25.1
XIAP-caspase, PFF	3.519×10^{12}	5.600×10^{11}	0.002649	8.83
XIAP-antagonist, OPLS	1.993×10^{12}	3.172×10^{11}	0.01683	56.1
XIAP-antagonist, PFF	3.383×10^{12}	5.384×10^{11}	0.005841	19.5

IV. Conclusions

Interactions of XIAP-BIR3 with caspase-9 and a small antagonist have been studied with the fixed-charges OPLS-AA and polarizable force field (PFF). Energies of the complexes have been calculated as a function of distance. Effects of low-ultrasound irradiation on the strength of the complexes have been assessed with a mechanistic model. It has been found that the polarizable force field predicts steeper walls of the potential wells for the formation of the complexes. In the case of the caspase-9 complex with XIAP, the total energy of the complex formation is ca. 30–40 kcal/mol, as predicted by the both force fields. For the XIAP-antagonist complex, PFF predicts a more negative energy of complex formation, which is consistent with the experimental findings. Both OPLS-AA and PFF reproduce well the increase of the total energy followed by the energy drop, as the molecules are separated from each other in aqueous solution. In general, the results demonstrate that the polarizable force field employed not only is adequate in simulating protein–ligand complexes in solutions but also gives a prediction of a stronger success of the antagonist to the caspase-XIAP interactions.

Estimation of the effect of low-intensity ultrasound on the strength of the complexes demonstrates that the simple frequency resonance hypothesis for the ultrasound-induced reactivation of apoptosis is ruled out. However, the pressure created by the cavitation accompanying the ultrasound irradiation is found to be sufficient to destroy the caspase-9 inhibition and, as a result, is named as the most probable candidate for the mechanism of apoptosis reactivation. While the overall mechanistic model of the ultrasound-molecular complex interaction is crude, it permits a qualitative explanation of the experimentally observed phenomena.

Acknowledgment. This work was supported in part by the Central Michigan University Faculty Research and Creative Endeavors (FRCE) grant 48984.

References

(1) (a) Shi, Y. *Protein Sci*. 2004, *13*, 1979. (b) Shiozaki, E. N.; Chai, J.; Rigotti, D. J.; Riedl, S. J.; Alnemri, E. S.; Fairman, R.; Shi, Y. *Mol. Cell* **2003**, *11*, 519.

(2) (a) See, for example: (a) Igney, F. H.; Krammer, P. H. *Nat. Rev. Cancer* **2002**, *2*, 277. (b) Reed, J. C. *Nat. Rev. Drug Discovery* **2002**, *1*, 111. (c) Los, M.; Burek, C. J.; Stroh, C.; Benedyk, K.; Hug, H.; Mackiewicz, A. *Drug Discovery Today* **2003**, *8*, 67.

(3) (a) Takahashi, R.; Deveraux, Q.; Tamm, I.; Welsh, K.; Assa-Munt, N.; Salvesen, G. S.; Reed, J. C. *J. Biol. Chem.* **1998**, *273*, 7787. (b) Riedl, S. J.; Renatus, M.; Schwarzenbacher, R.; Zhou, Q. Sun, C., Fesik, S. W.; Liddington, R. C.; Salvesen, G. S. *Cell* **2001**, *104*, 791. (c) Holcik, M.; Gibson, H.; Korneluk, R. G. *Apoptosis* **2001**, *6*, 253–261.

(4) (a) Liu, Z.; Sun, C.; Olejniczak, E. T.; Meadows, R. P.; Betz, S. F.; Oost, T.; Herrmann, J.; Wu, J. C.; Fesik, S. W. *Nature* **2000**, *408*, 1004. (b) Shi, Y. *Cell Death Differ.* **2002**, *9*, 93. (c) Du, C.; Fang, M.; Li, Y.; Li, L.; Wang, X. *Cell* **2000**, *102*, 33. (d) Verhagen, A. M.; Ekert, P. G.; Pakusch, M.; Silke, J.; Vaux, D. L. *Cell* **2000**, *102*, 43. (e) Nikolovska-Coleska, Z.; Xu, L.; Hu, Z.; Tomita, Y.; Li, P.; Roller, P. P.; Wang, R.; Fang, X.; Guo, R.; Zhang, M.; Lippman, M. E.; Yang, D.; Wang, S. *J. Med. Chem.* **2004**, *47*, 2430. (f) Schimmer, A. D. *Cancer Res.* **2004**, *64*, 7183.

(5) Johns, L. D. *J. Athletic Training* **2002**, *37*, 291.

(6) Mitragotri, S. *Nat. Rev. Drug Discovery* **2005**, *4*, 255.

(7) Yu, T.; Wang, Z.; Mason, T. J. *Ultrason. Sonochem.* **2004**, *11*, 95.

(8) Kondo, T.; Feril, L. B. *J. Radiat. Res.* **2004**, *45*, 479.

(9) Mohamed, M. M.; Mohamed, M. A.; Fikry, N. M. *Ultrasound Med. Biol.* **2003**, *29*, 1635.

(10) Lagneaux, L.; Meulenaer, E. C.; Delforge, A.; Dejeneffe, M.; Massy, M.; Moerman, C.; Hannecart, B.; Canivet, Y.; Lepeltier, M.-F.; Bron, D. *Exp. Hematol.* **2002**, *30*, 1293.

(11) Yu, T.; Xiong, Z.; Chen, S.; Tu, G. *Ultrason. Somochem.* **2005**, *12*, 345.

(12) Wu, C. C.; Roberts, P. H. *Phys. Rev. Lett.* **1993**, *70*, 3424.

(13) Pecha, R.; Gompf, B. *Phys. Rev. Lett.* **2000**, *84*, 1328.

(14) Cornell, W.; Cieplak, P.; Bayly, C.; Gould, I.; Merz, K.; Ferguson, D.; Spellmeyer, D.; Fox, T.; Caldwell, J.; Kollman, P. *J. Am. Chem. Soc.* **1995**, *117*, 5179.

(15) Halgren, T. A. *J. Comput. Chem.* **1999**, *20*, 730. and references therein.

(16) Jorgensen, W. L.; Maxwell, D. S.; Tirado-Rives, J. *J. Am. Chem. Soc.* **1996**, *118*, 11225.

(17) Dang, L. X.; Chang, T.-M. *J. Chem. Phys.* **1997**, *106*, 8149.

(18) Kaminski, G. A.; Stern, H. A.; Berne, B. J.; Friesner, R. A. *J. Phys. Chem. A* **2004**, *108*, 621.

(19) For representative publications, see:(a) Liu, Y. P.; Kim, K.; Berne, B. J.; Friesner, R. A.; Rick, S. W. *J. Chem. Phys.* **1998**, *108*, 4739. (b) Yu, H. B.; Hansson, T.; van Gunsteren, W. F. *J. Chem. Phys.* **2003**, *118*, 221. (c) Jardon-Valadez, E.; Costas, M. E. *THEOCHEM* **2004**, *677*, 227. (d) Patel, S.; Brooks, C. L. *J. Comput. Chem.* **2004**, *25*, 1. (e) Maple, J. R.; Cao, Y. X.; Damm, W.; Halgren, T. A.; Kaminski, G. A.; Zhang, L. Y.; Friesner, R. A. *J. Chem. Theory Comput.* **2005**, *1*, 694.

(20) Kaminski, G. A. *J. Phys. Chem. B* **2005**, *109*, 5884.

(21) Kaminski, G. A.; Friesner, R. A.; Tirado-Rives, J.; Jorgensen, W. L. *J. Phys. Chem. B* **2001**, *105*, 6474.

(22) *Maestro version 5.0*; Schrödinger, Inc.: Portland, OR, 2002.

(23) Oost, T. K.; Sun, C.; Armstrong, R. C.; Al-Assaad, A.-S.; Betz, S. F.; Deckwerth, T. L.; Ding, H.; Elmore, S. W.; Meadows, R. P.; Olejniczak, E. T.; Oleksijew, A.; Oltersdorf, T.; Rosenberg, S. H.; Shoemaker, A. R.; Tomaselli, K. J.; Zou, H.; Fesik, S. W. *J. Med. Chem.* **2004**, *47*, 4417.

(24) *Impact version 3.6*; Schrödinger, LLC: Portland, OR, 2005.

(25) (a) See, for example: (a) Naruse, Y. *Biosystems* **2002**, *66*, 55. (b) Naruse, Y. *Jpn. J. Appl. Phys.* **2004**, *43*, 3629.

CT8000188